View Article Online / Journal Homepage / Table of Contents for this issue

# Lab on a Chip

Miniaturisation for chemistry, biology & bioengineering

www.rsc.org/loc

Volume 7 | Number 11 | November 2007 | Pages 1377–1612

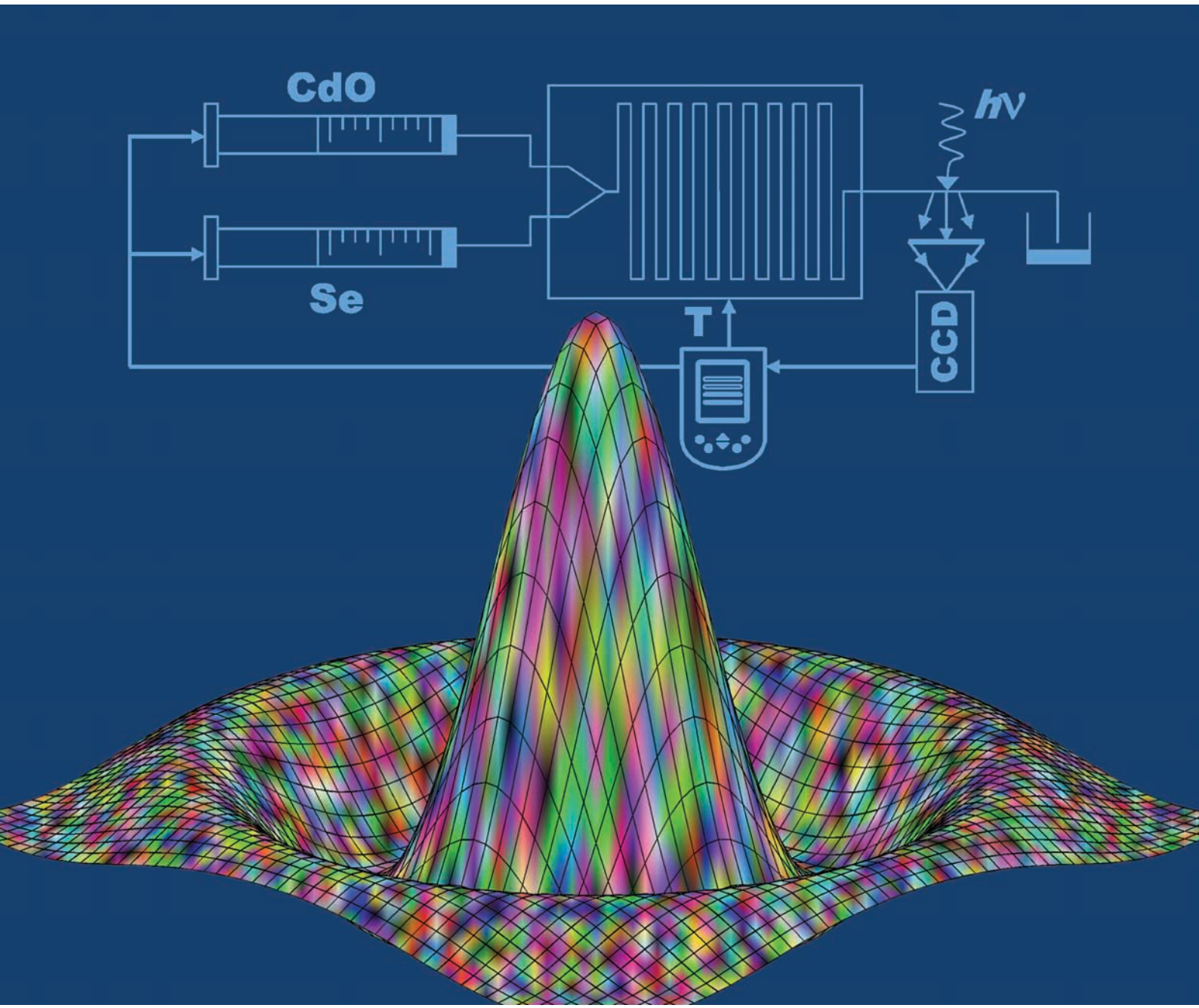


ISSN 1473-0197

Koster
Critical review of ESI MS for microfluidic applications

Beebe
Microfluidic logic gates

Whitesides
Pressure drop in bubble containing microchannels

deMello
Intelligent nanoparticle synthesis

RSC Publishing

1473-0197(2007)7:11;1-A

# Intelligent routes to the controlled synthesis of nanoparticles†

S. Krishnadasan,[a] R. J. C. Brown,[b] A. J. deMello[a] and J. C. deMello*[a]

*Received 25th July 2007, Accepted 3rd August 2007*
*First published as an Advance Article on the web 15th August 2007*
**DOI: 10.1039/b711412e**

Published on 15 August 2007. Downloaded by ETH-Zurich on 4/17/2019 7:46:01 PM.

We describe an autonomous 'black-box' system for the controlled synthesis of fluorescent nanoparticles. The system uses a microfluidic reactor to carry out the synthesis and an in-line spectrometer to monitor the emission spectra of the emergent particles. The acquired data is fed into a control algorithm which reduces each spectrum to a scalar 'dissatisfaction coefficient' and then intelligently updates the reaction conditions in an effort to minimise this coefficient and so drive the system towards a desired goal. In the tests reported here, CdSe nanoparticles were prepared by separately injecting solutions of CdO and Se into the two inlets of a heated y-shaped microfluidic reactor. A noise-tolerant global search algorithm was then used to efficiently identify—without any human intervention—the injection rates and temperature that yielded the optimum intensity for a chosen emission wavelength.

The difficulty of preparing nanoparticles in a controlled, reproducible manner is a key obstacle to the proper exploitation of many nanoscale phenomena.[1–4] An automated chemical reactor capable of producing (on demand at the point of need) high quality nanomaterials, with optimised physicochemical properties, would find numerous applications in nanoscale science and technology, especially in the areas of photonics,[5] optoelectronics,[6] bioanalysis[7–9] and targeted drug delivery.[10–12] Here, we investigate the feasibility of creating an autonomous system for synthesising CdSe quantum dots that, for a selected emission wavelength, emit with optimal intensity. Our approach builds on earlier work in which we proposed microfluidic reactors as favourable systems for nanoparticle synthesis, and showed that nanocrystalline CdS (n-CdS) prepared in microreactors exhibited improved monodispersity compared with n-CdS prepared in bulk.[13] In subsequent studies by ourselves and others, a variety of microfluidic architectures, based on continuous flow and droplet delivery schemes, have been used to prepare metal and compound semiconductor nanoparticles, including CdS, CdSe, $TiO_2$, Ag, Au, and Co.[14–34] In all cases, microfluidic procedures were found to offer advantages over bulk synthesis, most notably in the ability to fine tune the physical properties of the final product. Importantly, microfluidic devices permit the facile integration of in-line detectors for monitoring the particles as they form.[20,24] This raises the possibility of using control algorithms to 'intelligently' update the reaction conditions and so drive the system towards a desired goal, in principle enabling complete automation of the synthesis procedure.

[a]*Department of Chemistry, Imperial College London, South Kensington, London, UK SW7 2AZ. E-mail: j.demello@imperial.ac.uk*
[b]*Analytical Science Group, National Physical Laboratory, Hampton Road, Teddington, UK TW11 0LW*

† Electronic supplementary information (ESI) available: A summary of the parameters used by SNOBFIT, a schematic of the complete automated system (including the experimental set up and control algorithm), and a typical TEM image of the particles obtained using the automated system. See DOI: 10.1039/b711412e

Nanoparticles were prepared using the synthetic method of Peng and co-workers[35,36] by separately injecting precursor solutions of CdO and Se into the inlets of a heated y-shaped microfluidic chip (see Methods). The solutions mixed rapidly at the point-of-confluence, and nucleation and growth of the CdSe particles occurred along the reaction channel. The fluorescence spectra of the emergent particles were monitored using a 355 nm Nd:YAG laser and a CCD spectrometer. The y-shaped reactor provides three independent reaction parameters—the temperature ($T$), the injection rate of CdO ($F_{CdO}$) and the injection rate of Se ($F_{Se}$). The total injection rate ($F_{tot} = F_{CdO} + F_{Se}$) determines the mean residence time $\bar{\tau}$ on chip and the differential injection rate ($\gamma = F_{CdO}/F_{Se}$) determines the molar ratio $R$ of Cd to Se in the reaction mixture:

$$R = k\frac{F_{CdO}}{F_{Se}} \quad (1)$$

where $k$ = [CdO]/[Se] is the ratio of the molar concentrations of the two precursor solutions which, for the studies here, was 0.261.

The emission spectra typically comprise two main features (see, *e.g.* Fig. 2 inset): (i) a sharp Gaussian peak due to band-edge emission, with mean wavelength $\lambda_0$, full-width-half-maximum $\Delta\lambda$, and intensity $I_0$; and (ii) a broad feature at lower energies due to defect emission.[1,2,20] The effects on the emission spectra of varying $T$, $\bar{\tau}$ and $R$ are shown in the lowermost plots of Fig. 1a–c, respectively, and the effects on $\lambda_0$, $\Delta\lambda$ and $I_0$ are shown in the upper plots. Increasing the temperature and extending the reaction time have similar effects on the band-edge emission, leading in both cases to a red-shift and enhancement in the intensity. This is consistent with the formation at higher temperatures and longer reaction times of larger particles, in which excitons are less tightly constrained and so less susceptible to trapping at surface defects.[37,38] Increasing the Cd content from a large initial excess of Se leads to a red-shift of the band-edge emission up to $R$ = 0.5, followed by a blue-shift. The intensity varies in a similar way, peaking at a slightly higher value of $R$ = 0.8. The

 This journal is © The Royal Society of Chemistry 2007

Published on 15 August 2007. Downloaded by ETH-Zurich on 4/17/2019 7:46:01 PM.

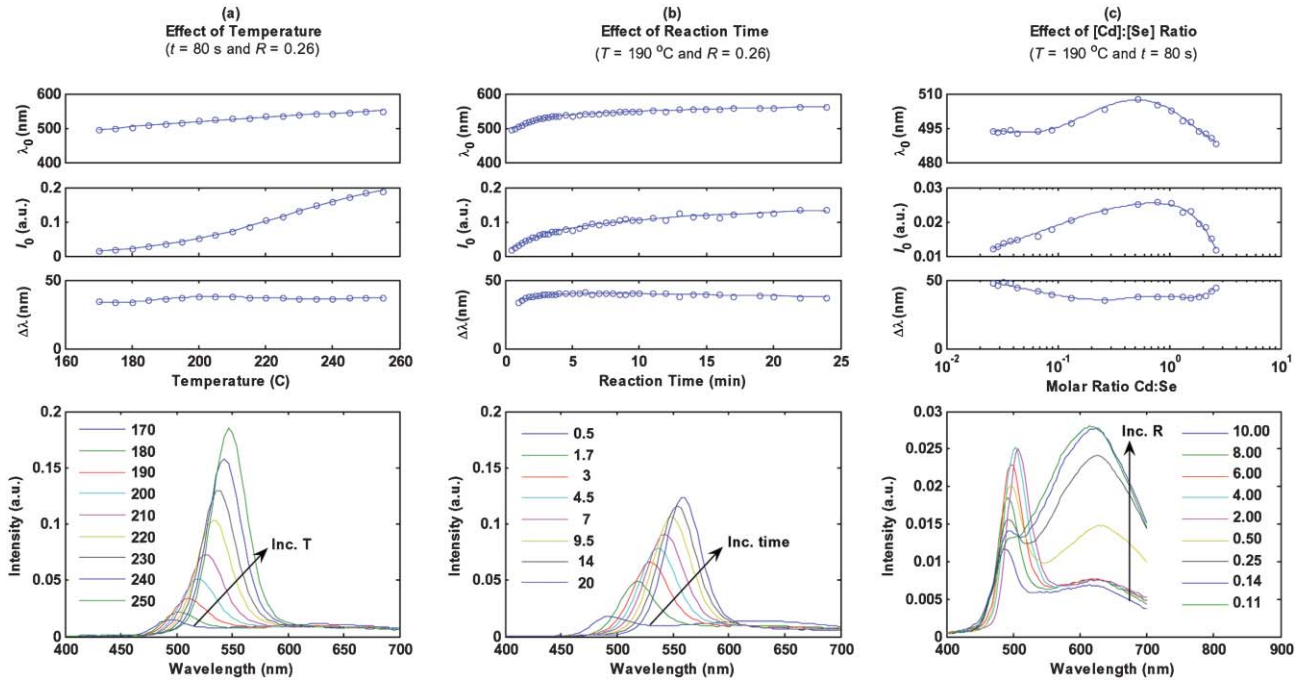


**Fig. 1** Graphs showing the variation of the emission characteristics with (a) temperature, (b) reaction time, and (c) Cd to Se ratio, holding in each case the other two reaction parameters constant. The emission spectra in the lowermost plots typically comprise a sharp Gaussian peak due to band-edge relaxation plus a broad low energy feature due to defects. The band-edge emission can be characterised in terms of the mean wavelength ($\lambda_0$), the peak intensity ($I_0$) and the full-width-half-maximum ($\Delta\lambda$), see inset to Fig. 2. The dependence of these parameters on the reaction conditions is shown in the uppermost plots.

defect emission is relatively weak in the excess Se regime, but increases rapidly beyond $R = 0.8$ and dominates the spectra when Cd is in substantial excess due to poor crystalline quality.[2]

Fig. 1a–c illustrate the systematic control over particle properties achievable in a microfluidic reactor but, collectively, represent a very limited data set. Just one reaction parameter was varied in each case, with the others being held fixed. (Formally, each plot corresponds to an arbitrary, orthogonal, one-dimensional [1D] slice through a three-dimensional [3D] hypersurface.) There is no guarantee similar behaviour would be obtained for different values of the fixed parameters. To obtain a detailed understanding of how the particle properties depend on the reaction conditions would require the entire 3D parameter space to be mapped out at finely spaced intervals in each direction. However, this would require many more measurements than is practical given typical time constraints. A preferable approach is to focus attention on regions of the parameter space where (for whatever reason) particles with desired properties are considered likely to be found at the expense of other less promising regions. One option is to use a response surface[39] to interpolate between previously tested reaction conditions and so identify promising locations for future measurements. The success of this approach depends on being able to judge where in the parameter space it is most profitable to sample, with it being important to strike an appropriate balance between local searching in the vicinity of identified optima and global searching in hitherto unexplored regions of the search space (where superior optima might potentially exist).

The control algorithm used here comprises two parts: (i) a utility function that assigns a scalar 'dissatisfaction coefficient' (DC) to the emergent particles based on their band-edge emission spectra; and (ii) an optimisation routine that seeks out the optimum reaction conditions as defined by the dissatisfaction coefficient. In this work, we use linear utility functions of the form:

$$u_\gamma(\gamma_c) = \frac{|\gamma_c - \gamma_t|}{|\gamma_w - \gamma_t|} \tag{2}$$

where $\gamma$ is the property under consideration and the subscripts c, t and w correspond to the current, target and worst possible outcomes, respectively. The dissatisfaction coefficient $u_\gamma(\gamma_c)$ runs linearly from zero for complete satisfaction (*i.e.* $\gamma_c = \gamma_t$) to one for complete dissatisfaction (*i.e.* $\gamma_c = \gamma_w$), enabling $\gamma_c$ to be optimised by straightforward minimisation of the utility function output. We begin by defining separate utility functions $u_\lambda$ and $u_I$ for the wavelength and intensity. In the case of $u_\lambda$, the target wavelength ($\lambda_t$) is the wavelength at which the particles are intended to emit, and the worst-case wavelength ($\lambda_w$) is either the shortest or longest accessible wavelength depending on whichever is furthest from $\lambda_t$ (and therefore represents the least favourable outcome). In the case of $u_I$, the target intensity ($I_t$) and the worst-case intensity ($I_w$) should ideally be set to the maximum and minimum intensities achievable for the target wavelength. These intensities are not known in advance, however, so we instead assign to $I_w$ and $I_t$ values of zero and $I^*$, respectively, where $I^*$ is an 'aspirational' value that substantially exceeds the maximum intensity we have ever measured at any wavelength. The two utility

Published on 15 August 2007. Downloaded by ETH-Zurich on 4/17/2019 7:46:01 PM.

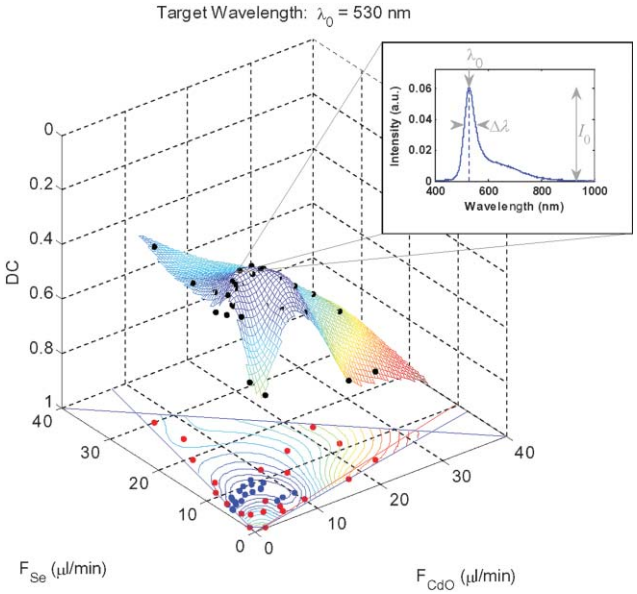


**Fig. 2** Graph showing the influence of the injection rates of CdO ($F_{CdO}$) and Se ($F_{Se}$) on the value of the dissatisfaction coefficient (DC) for a target wavelength of 530 nm and a fixed reaction temperature of 220 °C. The red line indicates a 1 : 1 ratio of Cd to Se in the reaction mixture and the blue lines define the flow rate constraints, namely $0.2 < F_{CdO}/F_{Se} < 5$ and 2 μl min$^{-1}$ $< F_{CdO} + F_{Se} <$ 40 μl min$^{-1}$. The red and blue markers show the specific reaction conditions sampled by the control algorithm, with the red and blue colours indicating corresponding DC values that are, respectively, greater or smaller than the median value of 0.26. The black markers denote the DC value at each point. An approximant surface has been superimposed on the data and the direction of the *z*-axis has been reversed to aid visualisation. The approximant is shown also as a contour map in the lowermost *xy*-plane. The spectrum corresponding to the smallest DC value of 0.190 is shown in the exploded graph, and it is clear that an exact match has been achieved to the target wavelength. The blue vertical dotted line denotes the target wavelength of 530 nm.

functions $u_\lambda$ and $u_I$ can be combined into a multi-attribute utility function $U(\lambda_c, I_c)$ that returns a single dissatisfaction coefficient based on $\lambda_c$ and $I_c$ jointly. Here, we use a simple weighted-product[40] of the form:

$$U(\lambda_c,I_c)=\frac{1}{k}(k\alpha u_\lambda(\lambda_c)+1)(k\beta u_I(I_c)+1)-\frac{1}{k} \quad (3)$$

where the weighting coefficients $\alpha$ and $\beta$ control the relative importance of $\lambda_c$ and $I_c$, and $k$ is a normalisation constant defined by $k = (1 - \alpha - \beta)/\alpha\beta$. Hence, $U(\lambda_c, I_c)$ may be written:

$$U(\lambda_c,I_c)=\frac{1}{k}\left(k\alpha\frac{|\lambda_c-\lambda_t|}{|\lambda_w-\lambda_t|}+1\right)\left(k\beta\frac{|I_c-I_t|}{|I_w-I_t|}+1\right)-\frac{1}{k} \quad (4)$$

The use of a utility function to characterise the output enables the overall physical process to be treated as a simple scalar mathematical function—the 'process function'—in which the reaction parameters are the inputs and the dissatisfaction coefficient is the output. The optimisation of the physical process is then formally equivalent to the minimisation of its associated process function. The optimisation, however, is complicated by several issues: (i) the mechanisms of nanoparticle formation (nucleation, growth, aggregation *etc.*) are poorly understood so no process models are available to guide the optimisation; (ii) most synthetic routes to nanoparticles usually take several minutes to complete so, from a practical perspective, relatively few process conditions can be evaluated during the search (typically <150); (iii) nanoparticle synthesis usually involves the optimisation of several properties at once, which creates multiple minima in the chemical parameter space; (iv) the process is invariably subject to noise (see *e.g.* Fig. 1); and (v) the reaction conditions must lie within strict limits, *i.e.* the parameter space is constrained. In a formal sense, these issues mean the optimisation routine must be capable of performing *constrained global optimisation of expensive noisy black-box functions*. This is a formidable numerical challenge, and it is only recently that effective algorithms have been developed to meet this goal. Here we use the routine Stable Noisy Optimisation by Branch and Fit by Huyer and Neumaier,[41] which works by first dividing the search space into a set of boxes that each contain one sampled data point, and then forming quadratic models around each point; local searching is handled by selecting the model minima as new evaluation points, and global searching by making measurements in large boxes (which correspond to large regions of unexplored territory). A summary of the parameters used by SNOBFIT plus a schematic of the complete system, including the experimental set up and control algorithm, is included as ESI. (Also included in the ESI is a typical TEM image of the particles obtained using the automated system.)†

To evaluate the efficacy of our numerical approach, we first consider a two dimensional [2D] chemical optimisation, in which the flow rates of the Se and Cd precursor solutions are independently tuneable but the temperature is held fixed. Our goal is to identify the reaction conditions that maximise the emission intensity for a specified target wavelength (TW), *i.e.* our primary objective is to achieve a 'close' match to $\lambda_t$ (defined here as a deviation of less than one nanometre) and our secondary objective is to maximise the emission intensity. This is achieved by using the empirically determined values $\alpha$ = 0.6 and $\beta$ = 0.2 in eqn (4), thereby placing greatest emphasis on the wavelength component whilst still allowing the intensity component to have a significant effect.

Here, we describe the results obtained for an arbitrary target wavelength of 530 nm but similar results were obtained for other TWs in the range 500 to 550 nm (Table 1). The lower and upper limits for the total flow rates were set to 2 and 40 μl min$^{-1}$, corresponding to mean reaction times of 501 and 25 s, respectively. The maximum differential between the injection rates of the two precursor solutions was set to five, *i.e.* $0.2 < \gamma < 5$, corresponding to Cd : Se ratios in the range 0.0523 to 1.30. The temperature was fixed at 220 °C. The algorithm was started 'cold', *i.e.* with no prior information, and it was allowed to perform ~40 trial measurements during the search. The flow rates sampled by the algorithm are indicated by the red and blue markers in the lowermost *xy*-plane of Fig. 2. (The significance of the colours and the contour lines is discussed below.) The blue lines represent the four flow rate constraints, which collectively define a trapezoidal-shaped parameter space. The red-line denotes a flow rate differential of $\gamma$ = 3.83 which gives a 1 : 1 ratio of Cd

 This journal is © The Royal Society of Chemistry 2007

**Table 1** Table summarising results obtained for 2D optimisation with different target wavelengths[a]

| Target/nm | $N_{meas}$ | $F_{CdO}$/μl min$^{-1}$ | $F_{Se}$/μl min$^{-1}$ | $T$/°C | $R$ = Cd/Se | DC | $N^*$ | $\lambda_0$/nm | $I_0$/a.u. | $\lvert\lambda_0 - \lambda_t\rvert$/nm |
|---|---|---|---|---|---|---|---|---|---|---|
| 500 | 43 | 22.470 | 4.510 | 220 | 1.30 | 0.19 | 33 | 499.9 | 0.080 | 0.1 |
| 510 | 43 | 15.420 | 15.020 | 220 | 0.27 | 0.19 | 38 | 510.1 | 0.040 | 0.1 |
| 520 | 43 | 5.980 | 11.470 | 220 | 0.14 | 0.19 | 43 | 520.0 | 0.050 | 0.0 |
| 530 | 43 | 4.960 | 9.830 | 220 | 0.13 | 0.19 | 43 | 530.2 | 0.060 | 0.2 |
| 540 | 43 | 4.330 | 4.710 | 220 | 0.24 | 0.18 | 39 | 539.8 | 0.110 | 0.2 |
| 550 | 43 | 2.830 | 1.730 | 220 | 0.43 | 0.17 | 40 | 550.3 | 0.180 | 0.3 |

[a] $N_{meas}$ = number of measurements undertaken in search; $N^*$ = measurement number at which optimum found; $\lvert\lambda_0 - \lambda_t\rvert$ = absolute deviation of peak wavelength $\lambda_0$ (at optimum conditions) from target wavelength $\lambda_t$; all other symbols as defined in main text.

Published on 15 August 2007. Downloaded by ETH-Zurich on 4/17/2019 7:46:01 PM.

to Se in the reaction mixture. (The larger area of the Se-rich region to the left of the red line is due to the Se precursor being of a substantially higher concentration than the Cd precursor.)

The DC value at each point is indicated by the black markers in the central volume of Fig. 2, where the direction of the $z$-axis has been reversed for easier visualisation, and a thin-plate-spline approximant surface[42] has been superimposed onto the raw data as a guide to the eye. The response surface has a single optimum in the low flow rate region of the parameter space, with the smallest DC value of 0.190 being obtained at CdO and Se injection rates of 4.960 and 9.830 μl min$^{-1}$, respectively (corresponding to a Cd : Se ratio of ~1 : 8). The emission spectrum of the particles produced under these flow conditions is shown in the inset graph, and an excellent match to the TW of 530 nm has evidently been achieved. The spectra obtained under other flow conditions (see *e.g.* Fig. 3b) matched less closely with the TW and/or were less intense, vindicating the choice of utility function in eqn (4) and the specific values selected for $\alpha$ and $\beta$.

Insight into the behaviour of the control algorithm can be obtained by examining the variation of the DC value with the measurement number $N$ (Fig. 3a, black markers). The DC value fluctuates due to the optimisation routine's continual alternation between local and global searching: in the local phase, the parameter space is sampled preferentially in regions where the existing DCs are small, yielding new DCs that are typically small also; in the global phase, unexplored regions of the parameter space are sampled where the DCs tend to be large (but where superior, as yet undiscovered, minima might in principle exist). The DC therefore tends to alternate between small and large values as the routine switches between local and global searching. It is instructive to divide the data points into two groups according to whether their DC values lie above or below the median value of 0.26 (Fig. 3a, horizontal dotted line). The members of the 'large' and 'small' data sets are denoted in Fig. 2 by red and blue markers, respectively, and it is clear that the blue points are clustered tightly around the optimum. The preferential sampling about the optimum is also evident from the inset histogram of Fig. 3a which shows a clear bias towards low DC values.

The variation of $y_{best}$ with $N$ is shown by the red staircase function in Fig. 3a, where $y_{best}$ is defined as the lowest DC

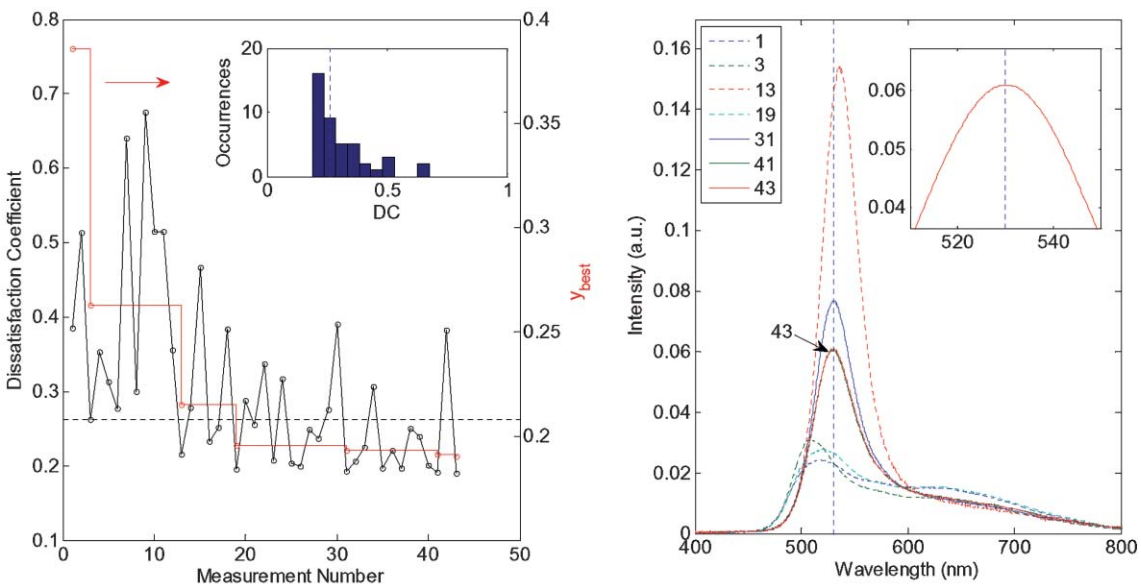


**Fig. 3** (a) The variation in DC value (black markers) and $y_{best}$ (red markers) with the measurement number $N$ for the data in Fig. 2. $y_{best}$, which corresponds to the lowest DC value in the existing data set, changes its value at $N$ = 3, 13, 19, 31, 41 and 43, signifying newly identified reaction conditions that are superior to those in the existing data set. The horizontal blue dotted line denotes the median DC value of 0.26. The inset histogram indicates a bias towards small DC values, indicating that the control algorithm spends a considerable time searching locally in the vicinity of the identified optimum. (b) The emission spectra at $N$ = 3, 13, 19, 31, 41 and 43. The spectra show a progressive improvement in terms of wavelength match and intensity as the DC value decreases. The inset shows a magnified image of the band-edge emission peak for measurement 43 with the vertical dotted line indicating the target wavelength.

Published on 15 August 2007. Downloaded by ETH-Zurich on 4/17/2019 7:46:01 PM.

value in the existing data set. $y_{best}$ changes value whenever the new reaction conditions yield particles with superior emission spectra to those in the existing data set. This happens at $N = 3$, 13, 19, 31, 41 and 43, and the corresponding emission spectra are shown in Fig. 3b. The values of $\alpha$ and $\beta$ in eqn (4) were selected to heavily penalise deviations from the TW and, consequently, spectrum 43 which coincides exactly with the TW (see Fig. 3b, inset) is rated superior to spectra 13, 19 and 31 which deviate by 1.5, 0.8 and 0.8 nm, respectively. (If desired, the utility function may be made more tolerant to wavelength deviations by increasing the value of $\beta$ relative to $\alpha$ in eqn 4.)

Importantly, from the shape of the response surface in Fig. 2, it seems unlikely that substantial further reductions in the dissatisfaction coefficient would be achieved through continued searching, implying the control algorithm has been able to locate the optimum conditions in just 43 measurements. This claim is arguably conjecture since some regions of the parameter space have been sampled only sparsely and, from a mathematical perspective, superior optima might exist in these unexplored regions. In fact this is very unlikely since the unexplored regions correspond to high flow rates which yield smaller particles that tend to emit shorter wavelength light of lower intensity. On physical grounds, we can therefore assert with considerable confidence that the global optimum has indeed been found. The optimisation was repeated with multiple TWs in the range 500 to 550 nm and, in each case, successful convergence was achieved within $\sim$40 measurements (Table 1).

The above measurements—which were performed 'blind' without any process model, pre-supplied data or human intervention—confirm the feasibility of automating nanoparticle synthesis. They relate however to a fairly simple 2D problem, in which only the precursor injection rates were varied and the temperature was held fixed, suggesting superior solutions might exist at other temperatures. To this end, we turn now to the full 3D optimisation, in which we again set the algorithm the task of producing particles that for a chosen wavelength emit with maximal intensity, but now permit the temperature to vary between 160 and 255 °C (whilst applying the same constraints to the flow rates). The algorithm was set the same TW of 530 nm and was again started cold. The number of measurements was set to a higher value of $\sim$100 due to the increased complexity of the task.

Fig. 4 shows a scatter plot of the sampled data, in which the marker locations indicate the reaction conditions and the colours denote the DC values (dark colours smaller). The wireframe 'cage' denotes the feasible space defined by the flow rate and temperature constraints, and the red lines indicate the flow conditions that yield a 1 : 1 balance of Cd and Se in the reaction mixture. The plot is somewhat crowded but the algorithm has evidently sampled certain regions of the parameter space preferentially—in particular the low flow rate zone at the foremost 'spine' of the cage and the high temperature zone towards the top. Dark blue data points are visible in several parts of the parameter space, indicating the existence of multiple optima.

The dissatisfaction coefficient is plotted against measurement number in Fig. 5a (black markers). The data again

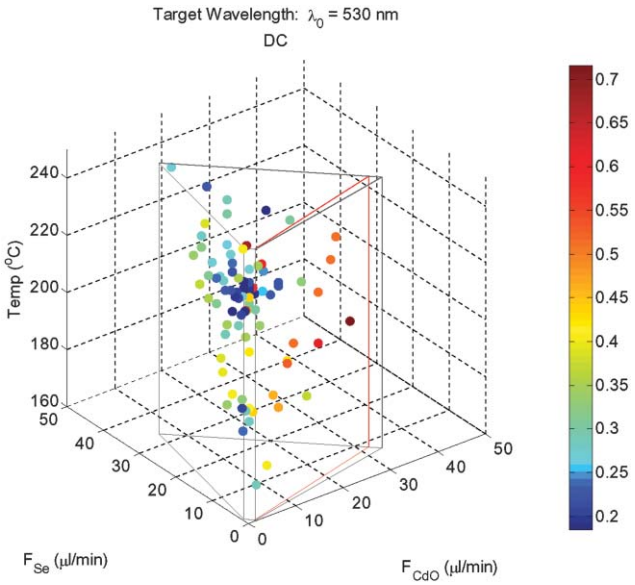


**Fig. 4** Scatter plot showing the influence of $F_{CdO}$, $F_{Se}$, and the temperature $T$ on the value of the dissatisfaction coefficient for the same target wavelength of 530 nm. The location of each data point indicates the temperature and flow rate conditions and the colour denotes the corresponding value of the dissatisfaction coefficient. The grey framework defines the flow rate and temperature constraints and the red lines indicate the flow conditions that yield a 1 : 1 ratio of Cd to Se in the reaction mixture.

fluctuates due to the alternation between local and global searching, and the inset histogram again indicates a clear bias towards low DC values. The red staircase function shows the variation of $y_{best}$ with $N$, and improvements occur at measurements 2, 6, 19, 21, 22, 27, 29, 35, 45 and 71. The corresponding emission spectra are shown in Fig. 5b. The spectra improve in terms of emission wavelength and intensity as the DC value gets smaller, with measurement 71 yielding the smallest DC value of 0.185 and an exact match to the wavelength (see inset). As anticipated, the DC value is slightly smaller than the value obtained for the 2D case.

The results obtained for other TWs in the range 500 to 550 nm are summarized in Table 2. The algorithm achieved an exact match to the TW (*i.e.* to within less than 1 nm) in all cases except 500 nm which yielded a 2.5 nm deviation from the TW. The reason for the small discrepancy in this case was due to the optimum conditions lying on the constraint boundary for the maximum flow rate. Convergence is inefficient when an optimum lies on a constraint boundary because the algorithm is able to sample on one side of the boundary only, and so obtains an incomplete picture of the local terrain. To obtain an exact match to the wavelength, it would have been necessary to increase the maximum number of samples (to compensate for the slower convergence) or to increase the maximum flow rate (to bring the optimum inside the constraint boundary and hence accelerate convergence).

The measurements in Tables 1 and 2 were performed alternately, *i.e.* for each TW the 2D and 3D optimisations were performed in immediate succession without changing the reagent solutions or otherwise disturbing the experimental system. The peak intensities in Tables 1 and 2 are therefore

 This journal is © The Royal Society of Chemistry 2007

Published on 15 August 2007. Downloaded by ETH-Zurich on 4/17/2019 7:46:01 PM.

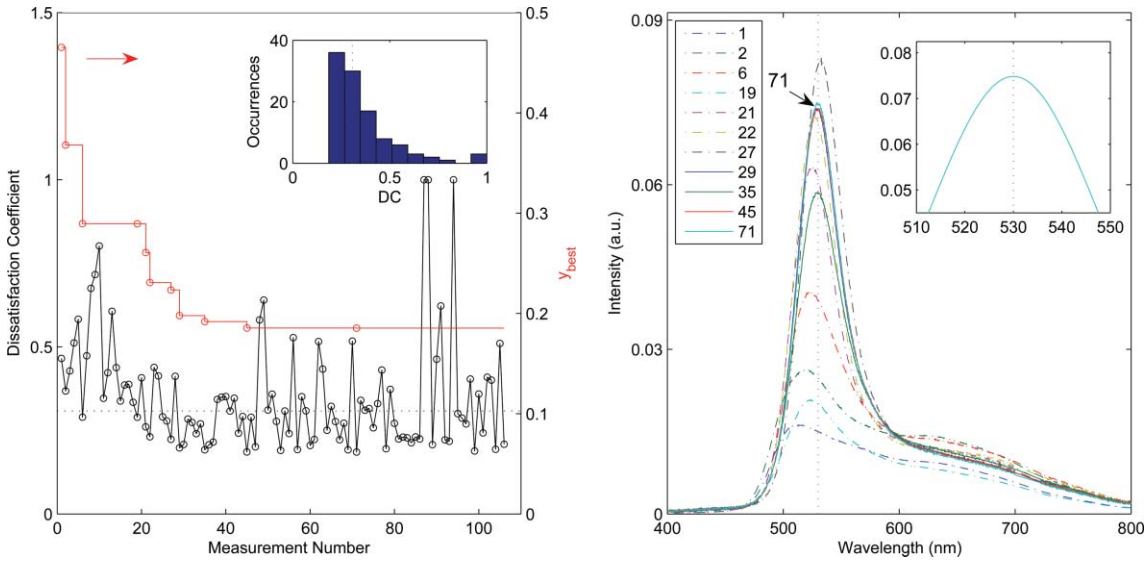


**Fig. 5** (a) The variation of the dissatisfaction coefficient (black markers) and $y_{best}$ (red markers) with the measurement number $N$ for the data in Fig. 4. The optimum DC value of 0.185 is obtained after 71 measurements. The horizontal blue dotted line denotes the median DC value of 0.31. The inset histogram again indicates a bias towards small DC values. $y_{best}$ changes at $N$ = 2, 6, 19, 21, 22, 27, 29, 35, 45 and 71, and the corresponding emission spectra are shown in (b). The spectra again show a progressive improvement in terms of intensity and wavelength-match as the DC value decreases. The inset shows a magnified image of the band-edge emission peak for measurement 71 with the vertical dotted line indicating the target wavelength.

**Table 2** Table summarising results obtained for 3D optimisation with different target wavelengths[a]

| Target/nm | $N_{meas}$ | $F_{CdO}$/μl min$^{-1}$ | $F_{Se}$/μl min$^{-1}$ | $T$/°C | $R$ = Cd/Se | DC | $N$* | $\lambda_0$/nm | $I_0$/a.u. | $\lvert\lambda_0 - \lambda_t\rvert$/nm |
|---|---|---|---|---|---|---|---|---|---|---|
| 500 | 106 | 31.920 | 7.980 | 241 | 1.05 | 0.21 | 72 | 502.5 | 0.090 | 2.5 |
| 510 | 106 | 3.040 | 0.760 | 172 | 1.05 | 0.19 | 106 | 510.3 | 0.060 | 0.3 |
| 520 | 106 | 17.290 | 7.410 | 236 | 0.61 | 0.18 | 106 | 519.9 | 0.080 | 0.1 |
| 530 | 106 | 8.230 | 10.770 | 228 | 0.20 | 0.19 | 71 | 530.0 | 0.070 | 0.0 |
| 540 | 106 | 3.040 | 0.760 | 209 | 1.05 | 0.17 | 61 | 540.6 | 0.210 | 0.6 |
| 550 | 106 | 3.040 | 0.760 | 237 | 1.05 | 0.12 | 60 | 549.6 | 0.420 | 0.4 |

[a] Symbols as defined for Table 1.

directly comparable. As anticipated, the 3D search consistently locates particles that emit with higher intensities. At shorter wavelengths, the gains are modest as the 2D measurements were performed at a relatively high temperature of 220 °C which tends to yield fairly high quality particles. At longer wavelengths, however, the improvement is substantial with the 3D optimization yielding an approximately two fold improvement relative to the 2D case. The fact that the algorithm requires just a hundred measurements to achieve this is encouraging and indicates the effectiveness of the control algorithm.

In conclusion, we have described an automated reactor for synthesising fluorescent CdSe quantum dots that, for a selected emission wavelength, emit with optimal intensity. The dots are prepared by the direct reaction of CdO and Se in a y-shaped microfluidic reactor. The emission spectra of the emergent particles are fed into a control algorithm which reduces each spectrum to a scalar dissatisfaction coefficient, and then updates the reaction conditions in an effort to minimise its value and so drive the system towards the desired outcome. The control algorithm uses a response surface to interpolate between existing data points and hence identify promising evaluation points. In some respects, this resembles the way in which a human operator would instinctively search for the optimum reaction conditions. The complexity of the task, however, increases rapidly as the parameter count increases. Hence, although it might be possible to manually identify the optimum for the 2D situation in Fig. 2, to do so for the 3D situation in Fig. 4 would prove substantially harder. Yet this is the exact challenge that synthesis chemists implicitly face in standard bench-top preparations (in which situation, moreover, they do not typically benefit from the control and 'dial-up' convenience of microfluidic reactors). In such circumstances, the probability of ending up in a non-global optimum—*i.e.* one that yields an exact match to the wavelength but delivers a sub-optimal intensity—is clearly high.‡

The approach described above is an important first step towards simplifying and automating nanoparticle production but there is still considerable scope for development, most

‡ This issue can be partially mitigated—at the expense of time and energy—by extended annealing of the final product at high temperatures to eliminate crystal defects and so improve quantum efficiencies. This, however, risks inducing changes in the emission wavelength. Alternatively, capping the CdSe core with a wide band-gap material can reduce the quenching effects of defects.

Published on 15 August 2007. Downloaded by ETH-Zurich on 4/17/2019 7:46:01 PM.

notably in its extension to more sophisticated chemistries and to core-shell and anisotropic nanostructures.[2,3,7,27,43–48] (In this work we have focused on the synthesis of fluorescent quantum dots, but the strategy has wider applicability to any particles (or other molecular species) whose properties can be monitored, directly or indirectly, in-line. In the case of non-fluorescent dots and rods, dynamic light scattering may prove an effective tool for controlling the size, aspect ratio and dispersity). The automation procedure is in principle applicable to any synthetic route that can be implemented in a microfluidic format, including both single- and multi-pot syntheses; we have, for instance, successfully applied it to a variety of single-source precursor routes based on metal-chalcogenide clusters. The key criterion for successful optimisation is the use of stable reagents and solvents that do not degrade or clog the channels in the course of the search for the optimal conditions. The algorithm itself makes no assumptions about the chemical system under optimisation, and the only specific changes needed in switching from one synthesis route to another are the number of reaction variables and the specific constraints applied to them. (The analysis of the acquired data and the optimisation logic remains the same irrespective of the synthesis route.) Once the optimum reaction conditions have been identified, the system can then be operated in this optimal state indefinitely provided the reactor and reagents do not degrade appreciably with time.

Finally, although the above results confirm the effectiveness of a simple utility function approach, it will be important to assess alternative multi-attribute optimisation techniques (*e.g.* goal seeking or hierarchical optimisation, see *e.g.* ref. 40) with a view to further improving efficiency and control. It would also be useful to develop heuristic termination criteria that allow the algorithm to assess when the global optimum has been found and the search can therefore end. Notwithstanding these challenges, we consider the general approach outlined above to offer a powerful route to the automated production of optimised nanoparticles which has the potential to transform the efficacy of nanoparticle synthesis in terms of control, yield and ease-of-use.

## Methods

Nanocrystalline CdSe was prepared by reacting CdO with Se using an adaptation to the method of Peng *et al.*[35,36] In short, a precursor Se solution was prepared by combining 30 mg of Se with 10 ml of 1-octadecene and 0.4 ml of trioctylphosphine and warming over a hot-plate. A Cd precursor solution was prepared by combining 13 mg of CdO and 0.6 ml of oleic acid in 10 ml of 1-octadecene and heating at 180 °C until clear. The reaction was performed in a glass y-shaped microfluidic chip with channels of width 330 μm and depth 160 μm. The reaction channel was 40 cm long and arranged in a serpentine architecture for compactness. The chip was placed on a stabilised hotplate with high spatial uniformity (Thickfilm Heater Watlow). The reaction was performed at temperatures in the range 160 to 255 °C. Two syringe pumps (PHD 2000, Harvard Instruments) were used to inject the precursor solutions into the inlet channels at rates up to 40 μL $min^{-1}$. The solutions mixed rapidly at the point-of-confluence, and nucleation and growth of the particles occurred along the reaction channel.

The emergent particles were monitored at ambient temperature at an observation zone down-stream of the reaction zone.[20] The particles were excited using a 355 nm solid-state laser (NanoUV 355, JDS Uniphase) and emission was detected using a fibre-optic CCD spectrometer (S2000, Ocean Optics). A fraction of the incident laser light was redirected to a Si photodiode using a beam-splitter, allowing the emission spectra to be corrected for variations in the laser intensity.

The experimental equipment (syringe pumps, hot-plate CCD-spectrometer *etc.*) were programmatically controlled using Labview Virtual Instruments, the control algorithm was implemented in Matlab, and data exchange between the two applications was handled using the MS Windows ActiveX component framework.

## References


1 C. D. Dushkin, S. Saita, K. Yoshie and Y. Yamaguchi, *Adv. Colloid Interface Sci.*, 2000, **88**, 37–78.
2 C. D. Donega, S. G. Hickey, S. F. Wuister, D. Vanmaekelbergh and A. Meijerink, *J. Phys. Chem. B*, 2003, **107**, 489–496.
3 C. N. R. Rao, V. V. Agrawal, K. Biswas, U. K. Gautam, M. Ghosh, A. Govindaraj, G. U. Kulkarni, K. R. Kalyanikutty, K. Sardar and S. R. C. Vivekchandi, *Pure Appl. Chem.*, 2006, **78**, 1619–1650.
4 G. G. Yordanov, G. D. Gicheva, B. H. Bochev, C. D. Dushkin and E. Adachi, *Colloids Surf., A*, 2006, **273**, 10–15.
5 T. Kawazoe, T. Yatsui and M. Ohtsu, *J. Non-Cryst. Solids*, 2006, **352**, 2492–2495.
6 I. Matsui, *J. Chem. Eng. Jpn.*, 2005, **38**, 535–546.
7 M. Green, *Angew. Chem., Int. Ed.*, 2004, **43**, 4129–4131.
8 M. N. Rhyner, A. M. Smith, X. H. Gao, H. Mao, L. L. Yang and S. M. Nie, *Nanomedicine*, 2006, **1**, 209–217.
9 J. M. Klostranec and W. C. W. Chan, *Adv. Mater.*, 2006, **18**, 1953–1964.
10 C. Medina, M. J. Santos-Martinez, A. Radomski, O. I. Corrigan and M. W. Radomski, *Br. J. Pharmacol.*, 2007, **150**, 552–558.
11 G. Han, P. Ghosh and V. M. Rotello, *Nanomedicine*, 2007, **2**, 113–123.
12 L. E. Euliss, J. A. DuPont, S. Gratton and J. DeSimone, *Chem. Soc. Rev.*, 2006, **35**, 1095–1104.
13 J. B. Edel, R. Fortt, J. C. deMello and A. J. deMello, *Chem. Commun.*, 2002, 1136–1137.
14 H. Nakamura, Y. Yamaguchi, M. Miyazaki, H. Maeda, M. Uehara and P. Mulvaney, *Chem. Commun.*, 2002, 2844–2845.
15 E. M. Chan, R. A. Mathies and A. P. Alivisatos, *Nano Lett.*, 2003, **3**, 199–201.
16 B. K. H. Yen, N. E. Stott, K. F. Jensen and M. G. Bawendi, *Adv. Mater.*, 2003, **15**, 1858–1862.
17 H. Z. Wang, X. Y. Li, M. Uehara, Y. Yamaguchi, H. Nakamura, M. P. Miyazaki, H. Shimizu and H. Maeda, *Chem. Commun.*, 2004, 48–49.
18 S. A. Khan, A. Gunther, M. A. Schmidt and K. F. Jensen, *Langmuir*, 2004, **20**, 8604–8611.
19 J. DeMello and A. DeMello, *Lab Chip*, 2004, **4**, 11N–15N.
20 S. Krishnadasan, J. Tovilla, R. Vilar, A. J. deMello and J. C. deMello, *J. Mater. Chem.*, 2004, **14**, 2655–2660.
21 I. Shestopalov, J. D. Tice and R. F. Ismagilov, *Lab Chip*, 2004, **4**, 316–321.
22 Z. L. Xue, A. D. Terepka and Y. Hong, *Nano Lett.*, 2004, **4**, 2227–2232.
23 M. Takagi, T. Maki, M. Miyahara and K. Mae, *Chem. Eng. J.*, 2004, **101**, 269–276.
24 E. M. Chan, A. P. Alivisatos and R. A. Mathies, *J. Am. Chem. Soc.*, 2005, **127**, 13854–13861.
25 H. Z. Wang, H. Nakamura, M. Uehara, Y. Yamaguchi, M. Miyazaki and H. Maeda, *Adv. Funct. Mater.*, 2005, **15**, 603–608.


 This journal is © The Royal Society of Chemistry 2007

Published on 15 August 2007. Downloaded by ETH-Zurich on 4/17/2019 7:46:01 PM.


26 J. Wagner and J. M. Kohler, *Nano Lett.*, 2005, **5**, 685–691.
27 J. R. Millman, K. H. Bhatt, B. G. Prevo and O. D. Velev, *Nat. Mater.*, 2005, **4**, 98–102.
28 J. M. Kohler, J. Wagner and J. Albert, *J. Mater. Chem.*, 2005, **15**, 1924–1930.
29 B. K. H. Yen, A. Gunther, M. A. Schmidt, K. F. Jensen and M. G. Bawendi, *Angew. Chem., Int. Ed.*, 2005, **44**, 5447–5451.
30 B. Yen, A. Gunther, M. Thalmann, M. G. Bawendi and K F. Jensen, in *Micro Total Analysis Systems 2004*, ed. T. Laurell, J. Nilsson, K. Jensen and D. J. Harrison, 2005, vol. 2, pp. 127–129.
31 J. Boleininger, A. Kurz, V. Reuss and C. Sonnichsen, *Phys. Chem. Chem. Phys.*, 2006, **8**, 3824–3827.
32 Y. J. Song, H. Modrow, L. L. Henry, C. K. Saw, E. E. Doomes, V. Palshin, J. Hormes and C. Kumar, *Chem. Mater.*, 2006, **18**, 2817–2827.
33 D. Shalom, R. C. R. Wootton, R. F. Winkle, B. F. Cottam, R. Vilar, A. J. deMello and C. P. Wilde, *Mater. Lett.*, 2007, **61**, 1146–1150.
34 B. F. Cottam, S. Krishnadasan, A. J. deMello, J. C. deMello and M. S. P. Shaffer, *Lab Chip*, 2007, **7**, 167–169.
35 Z. A. Peng and X. G. Peng, *J. Am. Chem. Soc.*, 2001, **123**, 183–184.
36 E. M. Boatman, G. C. Lisensky and K. J. Nordell, *J. Chem. Educ.*, 2005, **82**, 1697–1699.
37 M. A. Hines and P. Guyot-Sionnest, *J. Phys. Chem.*, 1996, **100**, 468–471.
38 M. G. Bawendi, P. J. Carroll, W. L. Wilson and L. E. Brus, *J. Chem. Phys.*, 1992, **96**, 946–954.
39 R. H. Myers, D. C. Montgomery, G. G. Vining, C. M. Borror and S. M. Kowalski, *J. Quality Technol.*, 2004, **36**, 53–77.
40 M. Zeleny, *Multiple Criteria Decision Making*, Mc-Graw Hill Book Company, New York, USA, 1982.
41 W. Huyer and A. Neumaier, http://www.mat.univie.ac.at/~neum/software/snobfit/.
42 J. Meinguet, *ZAMP*, 1979, **30**, 292–304.
43 A. C. C. Esteves and T. Trindade, *Curr. Opin. Solid State Mater. Sci.*, 2002, **6**, 347–353.
44 M. A. Malik, P. O'Brien and N. Revaprasadu, *Phosphorus, Sulfur Silicon Relat. Elem.*, 2005, **180**, 689–712.
45 T. Pellegrino, S. Kudera, T. Liedl, A. M. Javier, L. Manna and W. J. Parak, *Small*, 2005, **1**, 48–63.
46 S. Kalele, S. W. Gosavi, J. Urban and S. K. Kulkarni, *Curr. Sci.*, 2006, **91**, 1038–1052.
47 N. Revaprasadu and S. N. Mlondo, *Pure Appl. Chem.*, 2006, **78**, 1691–1702.
48 S. Kumar and T. Nann, *Small*, 2006, **2**, 316–329.